Simultaneous Conduction of Electronic Charge and Lithium Ions in Block Copolymers

Shrayesh N. Patel,[†,‡,§] Anna E. Javier,[†,§] Greg M. Stone,[‡,§] Scott A. Mullin,[†,§] and Nitash P. Balsara[†,‡,§,*]

[†]Environmental Energy Technologies Division, Lawrence Berkeley National Laboratory, Berkeley, California 94720, United States, [‡]Materials Sciences Division, Lawrence Berkeley National Laboratory, Berkeley, California 94720, United States, and [§]Department of Chemical and Biomolecular Engineering, University of California, Berkeley, California 94720, United States

ABSTRACT

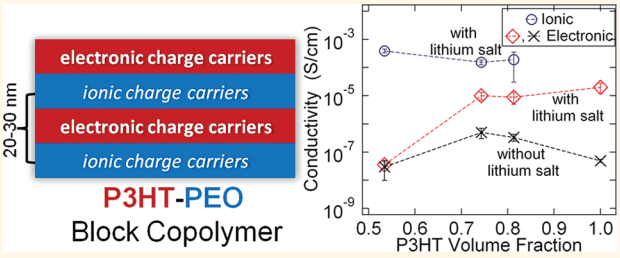

The main objective of this work is to study charge transport in mixtures of poly(3-hexylthiophene)-*b*-poly(ethylene oxide) (P3HT—PEO) block copolymers and lithium bis-(trifluoromethanesulfonyl) imide salt (LiTFSI). The P3HT-rich microphase conducts electronic charge, while the PEO-rich microphase conducts ionic charge. The nearly symmetric P3HT—PEO copolymer used in this study self-assembles into a lamellar phase. In contrast, the morphologies of asymmetric copolymers with P3HT as the major component are dominated by nanofibrils. A combination of ac and dc impedance measurements was used to determine the electronic and ionic conductivities of our samples. The ionic conductivities of P3HT—PEO/LiTFSI mixtures are lower than those of mixtures of PEO homopolymer and LiTFSI, in agreement with published data obtained from other block copolymer/salt mixtures. In contrast, the electronic conductivities of the asymmetric P3HT—PEO copolymers are significantly higher than those of the P3HT homopolymer. This is unexpected because of the presence of the nonelectronically conducting PEO microphase. This implies that the intrinsic electronic conductivity of the P3HT microphase in P3HT—PEO copolymers is significantly higher than that of P3HT homopolymers.

KEYWORDS: block copolymers · conducting polymers · mixed conductors · ac impedance · electronic conductivity · ionic conductivity

Electronic charges are usually transported in crystalline solids such as metals and semiconductors,[1−3] while ions are usually transported in aqueous or organic salt solutions. A significant problem in enabling redox reactions in a wide variety of systems such as batteries, fuel cells, and photoelectrochemical cells is the requirement that the active centers must be located at the junctions of pathways that transport electronic charge and ions. In lithium battery electrodes, for example, electronic conduction is enabled by the introduction of carbon, while ion conduction is enabled by the creation of a porous structure that is backfilled with an organic electrolyte.[4] Many of the active materials used in battery electrodes, such as $LiFePO_4$, are poor electronic and ionic conductors. In such cases, the active materials are made in the form of nanoparticles, which implies that pathways that conduct electrons and ions must lie within a few nanometers from each other. Identifying processing steps that lead to the presence of active materials at the junctions of the electron- and ion-conducting phases on these length scales is nontrivial. There is thus considerable interest in developing materials that conduct both electronic charge and ions on the nanometer length scales.

Simultaneous electronic and ionic conduction has been studied extensively in various inorganic materials.[5−10] In particular, Reiss has outlined methods for measuring electronic and ionic conduction for inorganic mixed conductors.[9,10] A method using ac impedance spectroscopy was developed to determine the presence of independent pathways for charge transport and resistance in an inorganic material between ion blocking electrodes.[11] In addition, some work has been done to model the impedance spectroscopy of mixed conductors, which included a term for accounting for imperfections in the electrodes.[12]

There also have been a few reports of simultaneous electronic and ionic conduction in various polymeric systems.[13−18] In refs 13 and 14, the authors studied conducting polymers, but were unable to decouple the electronic and ionic transport rates when both charges were present.

* Address correspondence to nbalsara@berkeley.edu.

Received for review November 23, 2011 and accepted January 27, 2012.

Published online February 10, 2012
10.1021/nn2045664

Ren *et al*. measured the electronic and ionic conductivity of poly(3-methylpyrrole-4-carboxylic acid) using dc and ac impedance measurements.[15] Plocharski studied the electronic and ionic conduction of doped poly(*p*-phenylene) homopolymer, but the source of ionic charges was not established.[17]

There is considerable interest in regioregular poly (3-hexylthiophene) (P3HT) due to its ability to conduct electronic charge.[19−22] The planarity of the polymer backbone is enabled by head-to-tail coupling of the thiophene monomer, and this promotes interchain $\pi-\pi$ interactions.[23] A nanofibrillar morphology, seen in both electron microscopy and atomic force microscopy, is believed to be a signature of these interactions.[22,24] Polythiophene and its derivatives are, however, semiconductors in their pristine form, and doping is necessary for the generation of charged carriers. Reported conductivity values for pristine regioregular P3HT range from 10^{-5} to 10^{-8} S/cm.[25−30] P3HT is a stable hole conductor (p-type semiconductor) when a dopant, such as I_2, is used to oxidize the thiophene unit, resulting in electronic conductivities of about 10 S/cm.[31,32] Electronic conductivity of P3HT films can also be increased by the application of electrochemical potentials in the presence of a liquid electrolyte.[33,34]

The McCullough group first showed that block copolymers comprising P3HT and insulating blocks self-assembled into conductive nanofibrils in a matrix of the insulating block.[32] They have reported this morphology in various block copolymers such as P3HT-*b*-polystyene,[35] P3HT-*b*-polyisoprene,[35] and P3HT-*b*-poly(methyl acrylate).[36] Highly doped P3HT-containing block copolymers with 40% P3HT by weight exhibit reported electronic conductivities as high as 2 S/cm.[37] The processing steps used to create the samples affect the observed morphology. Solution-cast samples made under rapid evaporation conditions result in highly disordered structures, while those made under slow evaporation conditions display the nanofibril morphology.[32] To our knowledge, there is only one report wherein traditional morphologies such as alternating lamellae and hexagonally packed cylinders are reported to form in P3HT-containing block copolymers.[38] The absence of these morphologies in most P3HT-containing block copolymers is attributed to the dominance of $\pi-\pi$ interactions and crystallization, the very effects that are responsible for electronic conduction in P3HT. This suggests that the self-assembly of P3HT-containing block copolymers is often kinetically trapped.[32]

The purpose of this paper is to study the relationship between morphology and charge transport in mixtures of P3HT−PEO block copolymers and lithium bis-(trifluoromethanesulfonyl) imide (LiTFSI). The P3HT block enables electronic transport, while the PEO block enables ion transport. Our results indicate that LiTFSI partitions into both P3HT and PEO microphases. The effect of this on charge transport is quantified. Our early results on this system have appeared in a brief communication.[39]

TABLE 1. Characteristics of Polymers Used in This Study

polymer name	$M_{n,P3HT}$[a] (kg/mol)	$M_{n,PEO}$[a] (kg/mol)	RR[b] (%)	ϕ_{HT}[c] (P3HT block)	PDI[d]
P3HT(5)	5.0		>94	1	1.2
P3HT−PEO(9−2)	9.0	2.0	>98	0.81	1.27
P3HT−PEO(6−2)	6.0	2.0	>95	0.74	1.33
P3HT−PEO(5−4)	5.0	4.2	>95	0.53	1.30

[a] M_n = number-average molecular weight, determined using ^{1}H NMR. [b] RR = regioregularity, determined using ^{1}H NMR. [c] Calculated using P3HT density[44] of 1.10 g/mL and PEO density[45] of 1.06 g/mL. [d] PDI = polydispersity index as determined by gel permeation chromatography with polystyrene standards.

Our group has studied the relationship between charge transport and morphology in lamellar block copolymers with an ion-conducting block and an insulating block.[40−43] These studies have shown that conductivity, σ, is proportional to the volume fraction of the conducting block, ϕ. We thus obtain

$$\sigma = f\phi\sigma_0 \quad (1)$$

where σ_0 is the intrinsic conductivity of the conducting phase and f is a factor that accounts for the morphology (also called tortuosity factor in the literature, although this term is usually used in the context of porous materials with ill-defined pores). For randomly oriented grains comprising alternating conducting and nonconducting lamellae, $f = 2/3$. The maximum value of f is obviously unity. This limit is appropriate when transport limitations at grain boundaries are not significant.[40] Equation 1 can readily be applied to systems wherein more than one kind of charge is transported. A major objective of the present study is to test the applicability of such a framework to P3HT−PEO/LiTFSI blends. To our knowledge, this is the first attempt to quantify the relationship between morphology and simultaneous transport of electronic and ionic charges.

RESULTS AND DISCUSSION

The characteristics of the P3HT homopolymer and the P3HT−PEO block copolymers and our nomenclature are summarized in Table 1. Figure 1a shows the small-angle X-ray scattering (SAXS) intensity, I, *versus* magnitude of the scattering vector, q, of P3HT−PEO-(9−2) at 90 °C in the absence and presence of salt at $r_0 = 0.085$, where r_0 is the molar ratio of lithium ions to ethylene oxide moieties. The neat sample ($r_0 = 0$) produces a featureless scattering profile. However, with the addition of salt, the scattering profile shows a broad primary peak at $q = q^* = 0.29$ nm^{-1} corresponding to a characteristic periodic length scale, $d = 22$ nm ($d = 2\pi/q^*$), and another broad peak at $q = 0.50$ nm^{-1}. Similar data are obtained from P3HT−PEO(6−2), as shown in

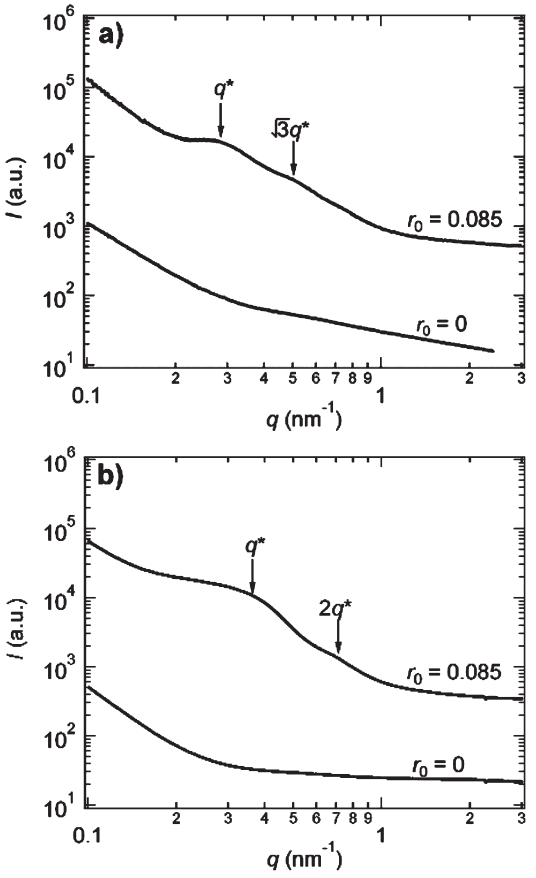

Figure 1. (a) SAXS of P3HT−PEO(9−2) and (b) P3HT−PEO-(6−2) at 90 °C. The SAXS profile at $r_0 = 0$ is featureless, while the addition of LiTFSI ($r_0 = 0.085$) indicates the presence of microphase separation. The features shown here are seen at all temperatures from 28 to 160 °C.

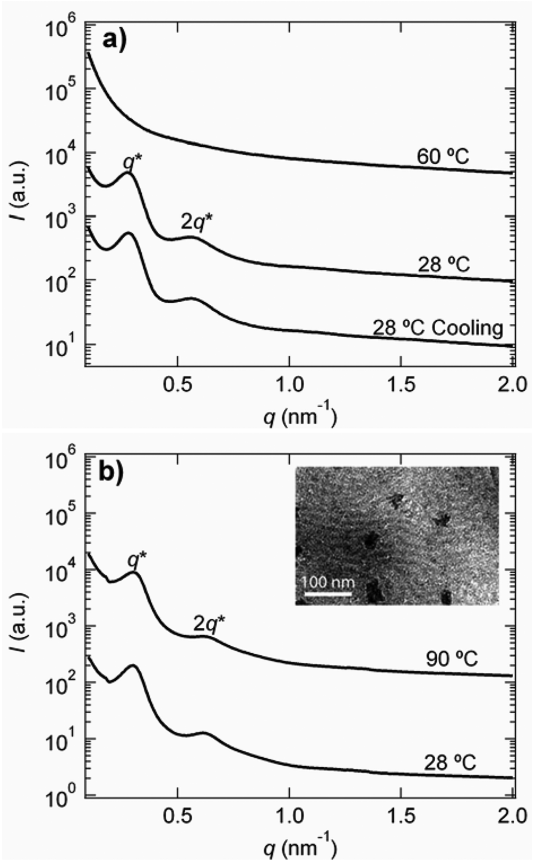

Figure 2. (a) SAXS of P3HT−PEO(5−4) at $r_0 = 0$. A lamellar microstructure is seen at 28 °C, while the featureless profile is obtained at 60 °C. The lamellar microstructure returns after cooling to 28 °C. (b) SAXS of P3HT−PEO(5−4) at $r_0 = 0.085$ indicating a lamellar microstructure. The inset shows the bright field transmission electron microscopy (TEM) image of a P3HT−PEO(5−4) $r_0 = 0.085$. Contrast in the image arises from density differences between the P3HT-rich (dark) and PEO with LiTFSI (light) microphases.

Figure 1b. The SAXS profile of neat P3HT−PEO(6−2) at 90 °C is featureless, but the addition of salt at $r_0 = 0.085$ results in broad peaks at $q^* = 0.37$ nm^{-1} and $q = 0.74$ nm^{-1}, corresponding to $d = 17$ nm. The broad peaks seen in Figure 1 are not characteristic of traditional block copolymer morphologies and are thus likely to be indications of the often-reported nanofibrillar morphology in P3HT-containing block copolymers.

Dramatically different results are obtained from neat P3HT−PEO(5−4) as shown in Figure 2a. At room temperature, the SAXS profile contains a primary peak at $q^* = 0.28$ nm^{-1} and a higher order peak at $2q^*$ indicative of a lamellar phase corresponding to a domain spacing, d (the center-to-center distance between adjacent PEO lamellae), of 22.5 nm. A featureless SAXS profile is obtained when the sample temperature is increased to 60 °C, indicating the disappearance of the lamellar morphology. The lamellar peaks return when the sample is cooled to room temperature. The SAXS data suggest the presence of a reversible order-to-disorder phase transition in the neat P3HT−PEO-(5−4). It is not clear if the high temperature phase in P3HT−PEO(5−4) contains nanofibrils. In Figure 2b, we show the SAXS profile of P3HT−PEO(5−4) at $r_0 = 0.085$ at room temperature and 90 °C. At both temperatures we observe peaks at $q^* = 0.31$ nm^{-1} and $2q^*$, indicating the presence of a lamellar structure with $d = 20.3$ nm. The lamellar structure of P3HT−PEO(5−4) at $r_0 = 0.085$ was confirmed by TEM, as shown in the inset of Figure 2b. There is good agreement between the length scale of the periodic structure determined by SAXS and TEM (about 20 nm). It should be noted that the TEM sample was not stained; that is, the natural electron density contrast between P3HT and PEO in the presence of LiTFSI is responsible for the image. The TEM image contained isolated dark features, as shown in Figure 2b. This may be due to residual homopolymers or some other contaminant in our samples. TEM images of P3HT−PEO(6−2) and P3HT−PEO(9−2) did not contain any discernible features. The SAXS results for all P3HT−PEO block copolymers indicate that the addition of LiTFSI enhances the microphase separation (Figures 1 and 2). This is also true in polystyrene-*b*-poly(ethylene oxide) (PS−PEO) block copolymers.[40,43]

Figure 3 compares the wide-angle X-ray scattering (WAXS) profiles of the P3HT–PEO copolymers with those of a P3HT homopolymer at 90 °C, which is above the melting temperature of PEO. The WAXS profiles thus reflect the local structure of the P3HT crystals. All of the profiles are dominated by the (100) and (010) reflections of the P3HT chains that are due to the side-chain spacing and $\pi-\pi$ stacking, respectively. Weaker peaks and shoulders corresponding to the (200) and (300) reflection are also seen in all of the samples. Qualitatively similar behavior is seen when salt is added to the P3HT–PEO block copolymers. The WAXS data suggest that the introduction of the PEO block and the addition of LiTFSI salt do not have a significant effect on the local arrangement of the P3HT segments. Interestingly there is no difference in the WAXS data from samples that contained nanofibrils [*e.g.*, P3HT–PEO(6–2)] and those that did not [P3HT–PEO(5–4)].

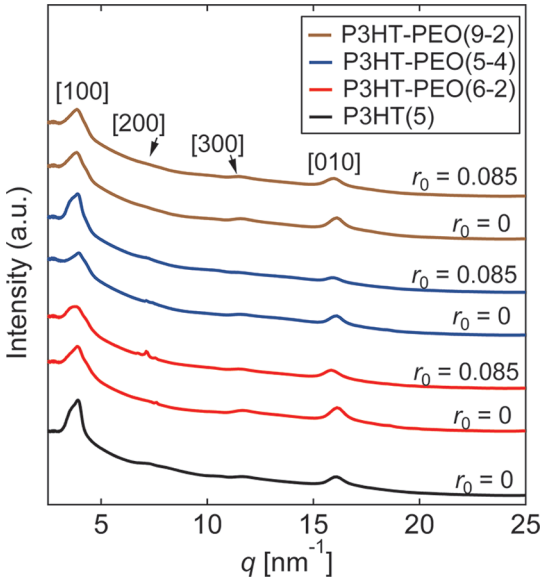

Figure 3. WAXS at 90 °C for P3HT(5) at $r_0 = 0$ (no LiTFSI) and P3HT–PEO at $r_0 = 0$ and $r_0 = 0.085$. The (100), (200), and (300) peaks correspond to the side-chain packing, while the (010) peak corresponds to the $\pi-\pi$ stacking. No diffraction peak is seen for PEO, as the samples are above the PEO melting point.

In Figure 4a, we show the results of impedance spectroscopy experiments on P3HT(5) sandwiched between nickel electrodes at 90 °C. The impedance data show one semicircle. The equivalent circuit used to analyze these data is a parallel combination of a resistor and CPE (constant phase element). Extrapolating the semicircle in Figure 4a to the real axis gives the electronic resistance of P3HT(5). It is reasonable to assume that the transport in this sample is dominated by electronic charge, and we thus obtain the electronic conductivity of P3HT(5), σ_{HT}, of $(4.9 \pm 0.6) \times 10^{-8}$ S/cm. This value is within the range of reported conductivity values of undoped regioregular P3HT (10^{-5} to 10^{-8} S/cm).[25−30] Our measured σ_{HT} is at the lower end of the range of the published data. Lui *et al*. found that in-plane conductivity of regioregular P3HT was 10^{-5} S/cm, while that in the through-plane geometry was 10^{-8} S/cm.[28] Our measurements were performed using a through-plane geometry. Differences in sample preparation must also be accounted for when comparisons between reported literature values are made. All of our measurements were made on freeze-dried, bulk samples.

In Figure 4b we show the Nqyuist plot of PEO homopolymer (M_n = 2 kg/mol) with LiTFSI at r_0= 0.085. As is typically the case with ion-conducting polymers, we see a single semicircle at high frequencies and a capacitive tail at low frequencies. Standard analysis using the equivalent circuit shown in Figure 4b results in the conclusion that the ionic conductivity of PEO, σ_{EO}, at $r_0 = 0.085$ is 2.05×10^{-3} S/cm. It should be noted that the semicircle approaches the Z' axis at a frequency of about 1 kHz, which is significantly higher than the semicircle touchdown of P3HT(5) (Figure 4a), where it is in the mHz range. The capacitive tail appears in Figure 4b but not in Figure 4a because nickel is a blocking electrode for ions but not for electronic charges. The lack of a capacitive tail is a clear indication of the presence of pathways for the transport of electronic charge. The presence of one semicircle in both Figure 4a and b is a signature of the presence of a single dominant pathway for charge transport in both P3HT and PEO homopolymers.

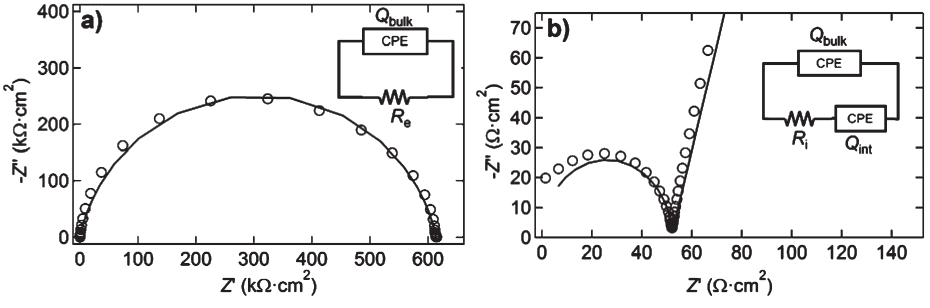

Figure 4. (a) Nyquist impedance plot ($-Z''$ *vs* Z') for P3HT(5) at 90 °C for frequency range of 1 MHz to 10 mHz. Fit parameters for P3HT(5) are $Q_{bulk} = 7.33 \times 10^{-11}$ F·s^{a-1}, $a_{bulk} = 0.875$, and $R_{e,fit} = 610$ kΩ·cm^2. (b) Nyquist impedance plot ($-Z''$ *vs* Z') for PEO at $r_0 = 0.085$ at 90 °C for frequency range of 1 MHz to 100 mHz. Fit parameters for PEO are $Q_{bulk} = 9.32 \times 10^{-10}$ F·s^{a-1}, $a_{bulk} = 1$, $Q_{int} = 3.14 \times 10^{-6}$ F·s^{a-1}, $a_{int} = 0.891$, and $R_{i,fit} = 52.2$ Ω·cm^2. The open circles correspond to the experimental data, and the solid curves correspond to the fit using the equivalent circuit shown in the inset.

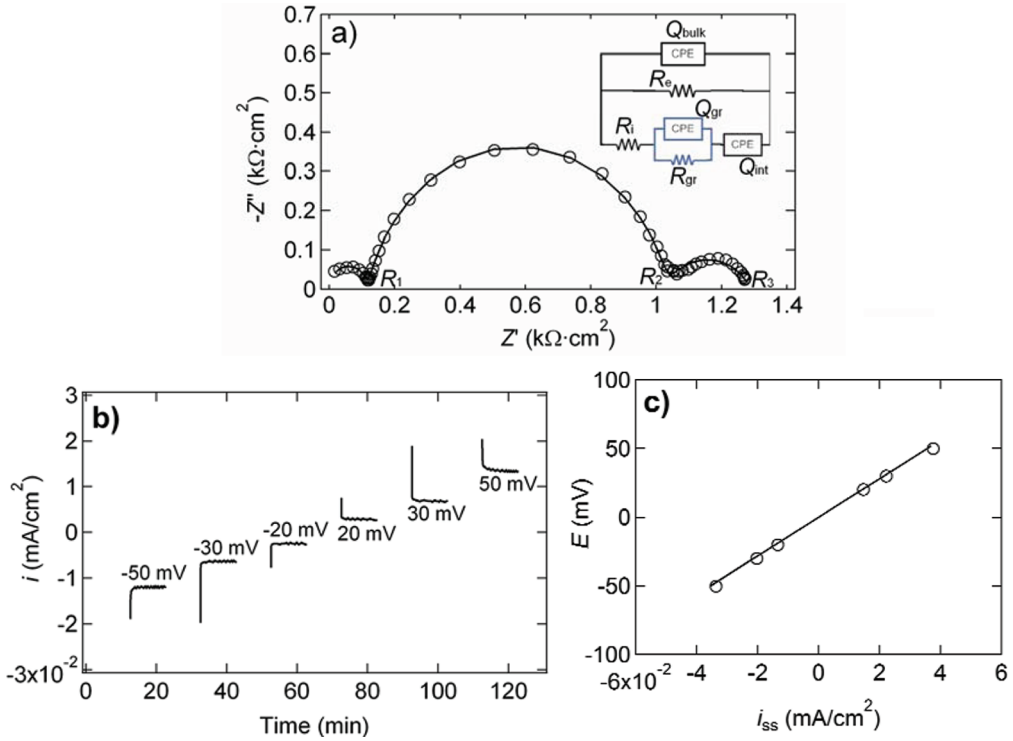

Figure 5. (a) Nyquist impedance plot ($-Z''$ *vs* Z') for P3HT−PEO(6−2)/LiTFSI (open circles) and the corresponding fit (solid curve) using the proposed equivalent circuit shown in the inset. Fit parameters: $Q_{bulk} = 3.79 \times 10^{-10}$ F·s^{a-1}, $a_{bulk} = 1$, $Q_{int} = 2.51 \times 10^{-5}$ F·s^{a-1}, $a_{int} = 0.658$, $Q_{gr} = 2.17 \times 10^{-7}$ F·s^{a-1}, $a_{gr} = 0.853$, and $R_{i,fit} = 0.129$ kΩ·cm^2, $R_{e,fit} = 1.29$ kΩ·cm^2, $R_{gr,fit} = 4.90$ kΩ·cm^2. (b) Current density (i) *vs* time curves at different applied dc potentials (E). (c) Corresponding Ohm's law plot of dc potential (E) *vs* steady-state current density (i_{ss}). Open circles are the experimental data, and solid line is the Ohm's law fit. The dc resistance, R_{dc}, from Ohm's law fit is 1.30 kΩ·cm^2.

Figure 5a shows impedance spectroscopy data from the P3HT−PEO(6−2)/LiTFSI mixture at $r_0 = 0.085$ sandwiched between nickel electrodes at 90 °C. The presence of three semicircles in Figure 5a, and the absence of such features in Figure 4a and b, suggests the presence of multiple charge transport pathways in the P3HT−PEO(6−2)/LiTFSI mixture. Again, the lack of a capacitive tail indicates the presence of continuous pathways for the transport of electronic charge. The total electronic resistance of the sample was determined from dc polarization experiments. A small dc potential was applied until a steady-state current was observed, as shown in Figure 5b. The corresponding resistance at steady state is the total electronic resistance because the nickel electrode blocks ions. In Figure 5c, the dc potentials are plotted *versus* steady-state current. The data follow Ohm's law, and the total electronic resistance of the sample, R_{dc}, is 1.30 kΩ·cm^2. This value is very close to the sum of the three semicircles in Figure 5a labeled as R_3. Therefore, extrapolation of the low-frequency semicircle to the Z' axis gives the total electronic resistance of the P3HT−PEO(6−2)/LiTFSI mixture.

As a first approximation, one may model the data from salt-containing P3HT−PEO copolymers (*e.g.*, Figure 5a) by proposing an equivalent circuit that is a linear combination of the equivalent circuits of the two constituent homopolymers. We expect the sample to contain bicontinuous ion- and electron-conducting channels, and thus the parallel combination of the two circuits is appropriate. Unfortunately, the equivalent circuit for this combination gives two Nyquist semicircles, which is inconsistent with the data in Figure 5a. The inset of Figure 5a shows the simplest equivalent circuit that is consistent with the data. The equivalent circuit comprises a parallel combination of an electronic and ionic conductor and an additional resistor/constant-phase-element circuit in series with the ionic conductor. This equivalent circuit gives three semicircles, consistent with the data in Figure 5a. Three semicircles have been reported before in inorganic mixed conductors, and in that case, the additional circuit has been attributed to the grain boundary resistance to either electronic or ionic transport.[11,46] Jamnik and Maier proposed that the middle semicircle reflects the fact that the electrodes are not completely reversible to the transfer of electronic charges.[12] The physical underpinning of the added circuit (the circuit in blue in Figure 5a inset) is uncertain. We will show that this limitation does not impede our ability to determine the overall electronic and ionic conductivity in our samples. The resistance and capacitance of the blue portion of the equivalent circuit in Figure 5a inset are referred to as R_{gr} and Q_{gr}. The equivalent circuit in

Figure 5a inset indicates that the high-frequency semicircle diameter, R_1, is the parallel combination of R_e and R_i.[11,12]

$$\frac{1}{R_1} = \frac{1}{R_i} + \frac{1}{R_e} \quad (2)$$

where R_e is the electronic resistance (also equal to R_3). This enables determination of R_i. The middle frequency range semicircle touchdown in Figure 5a can be used to calculate R_{gr} with the following equation:[11]

$$\frac{1}{R_2} = \frac{1}{R_i + R_{gr}} + \frac{1}{R_e} \quad (3)$$

where R_2 is the Z' intercept of the second semicircle (not the radius of the semicircle). We do not use R_{gr} in the discussion below and only include this equation for completeness. The solid curve in Figure 5a is a fit of the data to the equivalent circuit in Figure 5a inset.

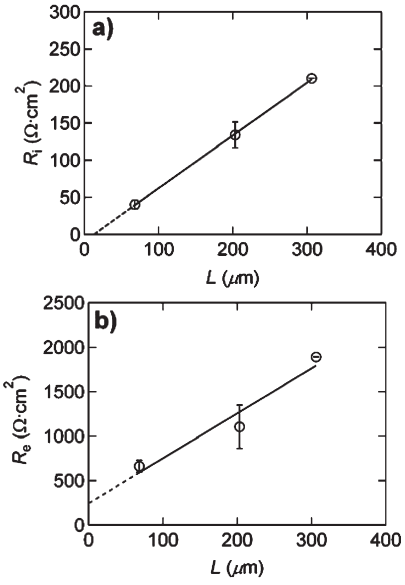

Figure 6. (a) Ionic resistance, R_i, and (b) electronic resistance, R_e, of P3HT−PEO(6−2) at r_0 = 0.085 at 90 °C as a function of sample thickness, L. Open circles are the experimental data, and solid line is a linear fit. The dashed line is the extrapolation of the linear fit to L = 0.

Not surprisingly, the two important parameters R_e and R_i obtained from the fit are consistent with those obtained by using eq 2.

The analysis described above was used on r_0 = 0.085 P3HT−PEO(6−2)/LiTFSI samples with different thicknesses. In Figure 6a and b we plot R_i and R_e thus obtained as a function of sample thickness, L. Both electronic and ionic resistance show approximately linear trends with thickness. In principle, the linear fits in Figure 6 should go through the origin. The y-intercept of the R_i *versus* L plot (−8 Ω·cm^2) is relatively small, while that of the R_e *versus* L plot (250 Ω·cm^2) is not. This may be due to errors intrinsic in extracting two independent resistances from the data or the presence of a non-negligible interfacial resistance to the transport of electronic charge at the electrode−polymer interface.

The remainder of this paper is based on data obtained from samples with L = 150−200 μm. In Figure 7a and b we show typical impedance data at 90 °C obtained from P3HT−PEO(9−2) and P3HT−PEO(5−4) with LiTFSI at r_0 = 0.085, respectively. The data contain three semicircles, and thus the method described above can be used to determine electronic and ionic conductivities of the samples. However, the relative magnitudes of the semicircles vary widely due to differences in R_i and R_e. The curves in Figure 7 are fits using the equivalent circuit shown in Figure 5a, inset, which enable determination of R_i and R_e. R_e is much greater than R_i for all three sample, implying that $R_1 \approx R_i$ (see eq 2).

Electronic and ionic conductivities of P3HT−PEO(9−2) and P3HT−PEO(6−2) at r_0 = 0.085 at selected temperatures were determined by the methods given above, and the results are shown in Figure 8. Both samples show an increase in σ_e and σ_i as temperature is increased from 40 to 90 °C. The temperature dependence on ionic conductivity is fitted to the Vogel−Tamman−Fulcher equation:

$$\sigma_i = A_i \exp\left(\frac{-E_i}{R(T - T_0)}\right) \quad (4)$$

where σ_i is the ionic conductivity, A_i is a pre-exponential factor proportional to the number of ionic charge

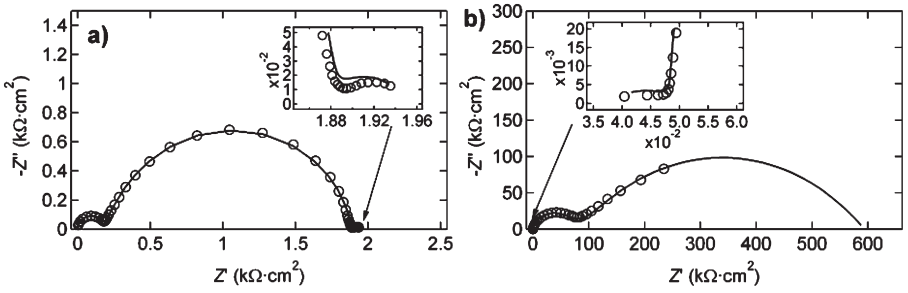

Figure 7. (a) Nyquist impedance plot ($-Z''$ *vs* Z') at 90 °C for P3HT−PEO(9−2) at r_0 = 0.085 with frequency range of 1 MHz to 5 mHz. Fit parameters: Q_{bulk} = 1.01 × 10^{-9} F·s^{a-1}, a_{bulk} = 1, Q_{int} = 6.46 × 10^{-6} F·s^{a-1}, a_{int} = 0.572, Q_{grb} = 2.07 × 10^{-7} F·s^{a-1}, a_{gr} = 0.925, and $R_{i,fit}$ = 0.195 kΩ·cm^2, $R_{e,fit}$ = 1.95 kΩ·cm^2, $R_{gr,fit}$ = 47.3 kΩ·cm^2. (b) Nyquist impedance plot ($-Z''$ *vs* Z') at 90 °C for P3HT−PEO(9−2) at r_0 = 0.085 with frequency range of 1 MHz to 1 mHz. Fit parameters: Q_{bulk} = 9.34 × 10^{-8} F·s^{a-1}, a_{bulk} = 0.912, Q_{int} = 2.02 × 10^{-5} F·s^{a-1}, a_{int} = 0.470, Q_{grb} = 5.0 × 10^{-7} F·s^{a-1}, a_{grb} = 0.422, and $R_{i,fit}$ = 0.053 kΩ·cm^2, $R_{e,fit}$ = 594 kΩ·cm^2, $R_{gr,fit}$ = 100 kΩ·cm^2. The open circles represent experimental data, while the solid curve represents the equivalent circuit fit.

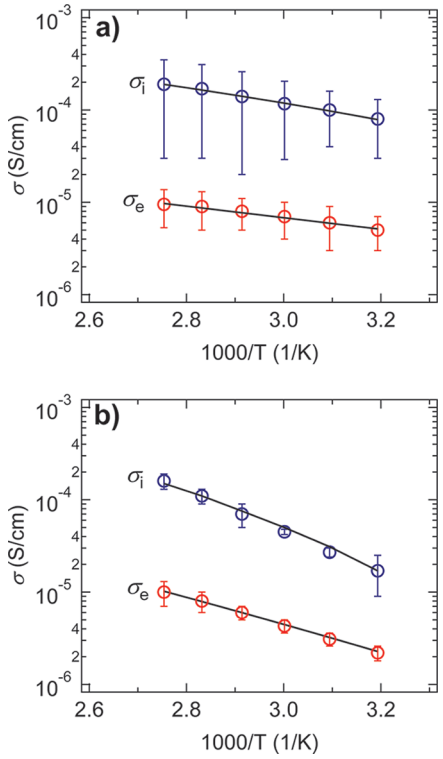

Figure 8. Temperature dependence of ionic and electronic conductivity for (a) P3HT−PEO(9−2) at r_0 = 0.085 and (b) P3HT−PEO(6−2) at r_0 = 0.085. Open symbols are experimental data, and solid curves are fits using the VTF and Arrhenius equations for ionic and electronic conductivities, respectively. The VTF fit parameters are $A_i = 1.63 \times 10^{-3}$ S/cm, E_i = 0.032 eV, and T_0 = 190K for P3HT−PEO(9−2) and A_i = 1.00 × 10^{-2} S/cm, E_i =0.066 eV, and T_0 = 200K for P3HT−PEO(6−2). The Arrhenius fit parameters are A_e = 5.14 × 10^{-4} S/cm and E_e = 0.125 eV, for P3HT−PEO(9−2), and A_e = 3.1 × 10^{-2} S/cm S/cm and E_e = 0.255 eV for P3HT−PEO(6−2).

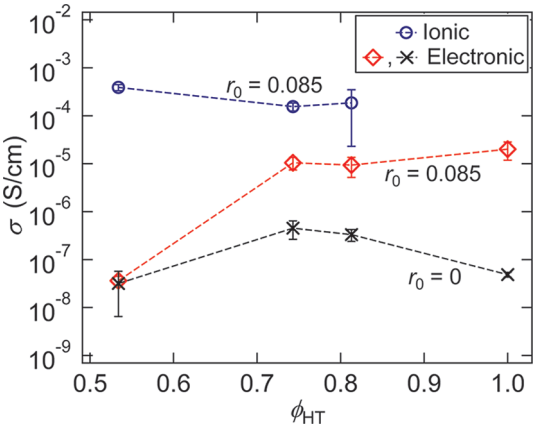

Figure 9. Electronic conductivity of P3HT homopolymer and P3HT−PEO block copolymers as a function of the P3HT volume fraction, ϕ_{HT}, at 90 °C. Measurements were made with (r_0 = 0.085) and without (r_0 = 0) added salt. The ϕ_{HT} values for the three block copolymers are given in Table 1. The ϕ_{HT} = 1 data set corresponds to homopolymer P3HT(5), and the salt concentration of 0.085 is actually r_{HT}. The ionic conductivities of the P3HT−PEO block copolymers were measured only with added salt (r_0 = 0.085). The dashed lines are guides for the eye.

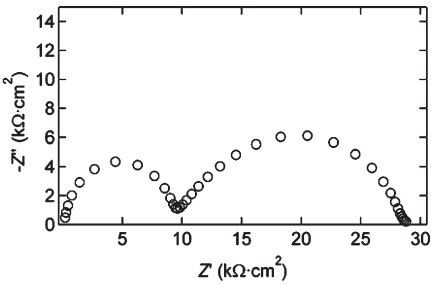

Figure 10. Nyquist impedance plot (−Z'' *vs* Z') at 90 °C for P3HT−PEO(6−2) at r_0 = 0. The Z' intercept of the rightmost semicircle gives the electronic resistance.

carriers, E_i is the pseudoactivation energy for ion motion, R is the gas constant, T is the temperature, and T_0 is a reference temperature, which is typically 25 K below the glass transition temperature of PEO.[47] We left T_0 as a fit parameter because the glass transition temperature of PEO changes with added salt. The temperature dependence on electronic conductivity was fit to the Arrhenius equation:

$$\sigma_e = A_e \exp\left(\frac{-E_e}{RT}\right) \quad (5)$$

where σ_e is the electronic conductivity, A_e is a pre-exponential factor, and E_e is the activation energy for electronic charge transport. The application of the Arrhenius model assumes the conduction mechanism is through thermally activated hopping, which is common for undoped semiconducting polymers.[48] The resulting fit parameters using eqs 6 and 7 are given in the caption of Figure 8.

To further analyze the electronic and ionic charge transport properties, we will focus on the data obtained at 90 °C. Figure 9 shows σ_e and σ_i of all three P3HT−PEO samples with and without LiTFSI. The ionic conductivity, σ_i, of P3HT−PEO(5−4) at r_0 = 0.085 is (3.9 ± 0.6) × 10^{-4} S/cm, which is the highest among the three block copolymer samples. This is not surprising, as this polymer has the highest PEO volume fraction. The ionic conductivities of P3HT−PEO(9−2) and P3HT−PEO(6−2) at r_0 = 0.085 are within experimental error, in spite of the difference in PEO volume fraction. The values of σ_i reported here are similar to the reported ionic conductivities of other PEO-containing block copolymers.[42] All of the previous data (*e.g.*, ref 42) on PEO-containing block copolymers are restricted to systems wherein the nonionically conducting block was insulating. The values of σ_e of P3HT−PEO(9−2) and P3HT−PEO(6−2) at r_0 = 0.085 are (9 ± 4) × 10^{-6} S/cm and (1.0 ± 0.3) × 10^{-5} S/cm. A significantly lower value of (3.6 ± 0.9) × 10^{-8} S/cm was obtained from P3HT−PEO(5−4) at r_0 = 0.085. The neat P3HT−PEO samples (r_0 = 0) exhibited impedance data that were similar to those obtained from P3HT−PEO/LiTFSI mixtures, but with two semicircles, as shown in Figure 10 for P3HT−PEO(6−2). The analysis described

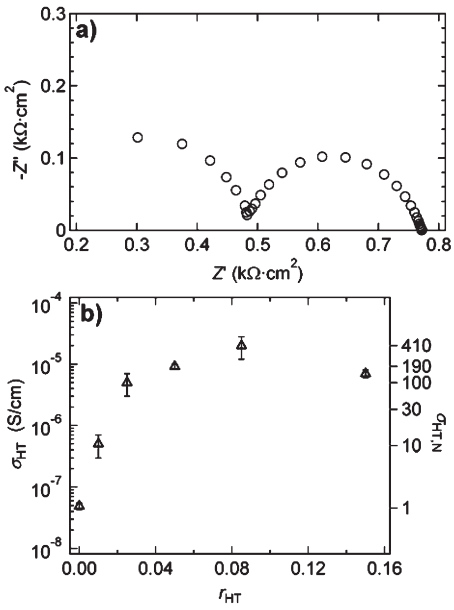

Figure 11. (a) Nyquist impedance plot ($-Z''$ *vs* Z') at 90 °C for a P3HT(5)/LiTFSI mixture with salt concentration r_{HT} = 0.085. The Z' intercept of the rightmost semicircle gives the electronic resistance. (b) Electronic conductivity, σ_{HT}, at 90 °C for P3HT(5)/LiTFSI salt mixtures at various salt concentrations. Right-hand axis corresponds to the normalized P3HT electronic conductivity, $\sigma_{HT,N}$ (relative to σ_{HT} at r_{HT} = 0), as defined by eq 6. These data are used to determine the partitioning of salt in the P3HT microphase as described in the text.

above holds for these samples, and the low-frequency Z' intercept gives R_e. The dc test showed that σ_e of neat P3HT−PEO(6−2) was $(4.4 \pm 0.3) \times 10^{-7}$ S/cm at 90 °C, which is in good agreement with σ_e of $(5 \pm 2) \times 10^{-7}$ S/cm from ac impedance spectroscopy. The effect of added salt on the electronic conductivities of the P3HT−PEO copolymers is shown in Figure 9. σ_e of P3HT−PEO(5−4) does not change appreciably when r_0 is increased from 0 to 0.085. One might anticipate this result if all of the added LiTFSI were preferentially located in the PEO microphase. In contrast, σ_e values of P3HT−PEO(9−2) and P3HT−PEO(6−2) increase by factors of 28.1 and 23.0 when r_0 is increased from 0 to 0.085, indicating that the electronic conductivity of the P3HT microphases is affected by LiTFSI.

The above observation motivated us to prepare several P3HT(5)/LiTFSI mixtures in the concentration range $0 \leq r_{HT} \leq 0.15$, where r_{HT} is the molar ratio of LiTFSI to 3-hexylthiophene monomer (refer to Experimental Methods section for details). The mixtures appeared homogeneous and with a clear red color when viewed by the naked eye (which could indicate the absence of chemical doping). Figure 11a shows the Nyquist plot of the P3HT(5)/LiTFSI mixture at r_{HT} = 0.085. It contains two semicircles with no capacitive tail, and thus the touchdown of the second semicircle gives the electronic resistance R_e, which was confirmed by dc measurements. In Figure 11b, we show the

TABLE 2. Estimated Values of LiTFSI Salt Concentrations in P3HT, r_{HT}, and in PEO, r_{EO}, for P3HT−PEO Salt Mixtures at r_0 = 0.085 and 90 °C

polymer name	r_{HT}	r_{EO}
P3HT−PEO(9−2)	0.017 ± 0.003	0.065 ± 0.003
P3HT−PEO(6−2)	0.016 ± 0.002	0.072 ± 0.001
P3HT−PEO(5−4)	0.0003 ± 0.0004	0.0849 ± 0.0001

TABLE 3. Normalized Ionic Conductivity, $\sigma_{i,N}$, and Electronic Conductivity, $\sigma_{e,N}$, for P3HT−PEO Salt Mixtures at r_0 = 0.085 and 90 °C

polymer name	$\sigma_{i,N}$	$\sigma_{e,N}$
P3HT−PEO(9−2)	0.6 ± 0.5	8 ± 2
P3HT−PEO(6−2)	0.33 ± 0.06	12 ± 5
P3HT−PEO(5−4)	0.48 ± 0.06	1.2 ± 0.9

electronic conductivity of P3HT(5)/LiTFSI mixtures, σ_{HT}, as a function of r_{HT} at 90 °C. σ_{HT} increases rapidly with increasing r_{HT} in the $r_{HT} \leq 0.04$ regime. The right-hand-axis in Figure 11b plots $\sigma_{HT,N}$ as a function of r_{HT}, where $\sigma_{HT,N}$ is the normalized electronic conductivity of P3HT(5)/LiTFSI, defined as the ratio of σ_{HT} at the r_{HT} of interest to σ_{HT} at r_{HT} = 0.

Returning to the electronic conductivity data in Figure 9, we make the simplifying assumption that the increase in electronic conductivity of the P3HT−PEO/LiTFSI mixtures relative to neat P3HT−PEO is due to mixing of some of the added LiTFSI with the P3HT. We define k for each of the block copolymers as

$$k = \frac{\sigma_e(r_0 = 0.085)}{\sigma_e(r_0 = 0)} \quad (6)$$

The values of k for P3HT−PEO(9−2), P3HT−PEO(6−2), and P3HT−PEO(5−4) are 28.1, 23.0, and 1.14, respectively. The concentration of LiTFSI in the P3HT microphase is obtained by determining the value of r_{HT} in Figure 11b where $\sigma_{HT,N} = k$. The LiTFSI concentrations in the P3HT microphase thus obtained are tabulated in Table 2. Also given in Table 2 are the inferred LiTFSI concentrations in the PEO microphase obtained by mass balance:

$$\frac{w_{EO}}{M_{0,EO}} r_0 = \frac{[1 - w_{EO}]}{M_{0,HT}} r_{HT} + \frac{w_{EO}}{M_{0,EO}} r_{EO} \quad (7)$$

where r_{EO} is the salt concentration in the PEO microphase, w_{EO} is the PEO microphase weight fraction, $M_{0,EO}$ is the PEO repeat unit molecular weight, and $M_{0,HT}$ is the P3HT repeat unit molecular weight. It is evident from Table 2 that about 20% of the added salt partitions into the P3HT microphases in samples P3HT−PEO(9−2) and P3HT−PEO(6−2). This suggests that LiTFSI has an affinity toward the P3HT microphases with the nanofibrillar morphology.

We define a normalized ionic conductivity,

$$\sigma_{i,N} = \frac{\sigma_i}{\phi_{EO}\sigma_{EO}(r_{EO})} \quad (8)$$

where ϕ_{EO} is the PEO volume fraction and $\sigma_{EO}(r_{EO})$ is the ionic conductivity of pure PEO homopolymer at a salt concentration of r_{EO} at the temperature of interest. If eq 1 was valid and the intrinsic conductivity of the PEO microdomains in the P3HT−PEO/LiTFSI mixtures was identical to σ_{EO}, then $\sigma_{i,N} = f_i$, the morphology factor for ionic conduction. The values of σ_{EO} used in the normalization were obtained at r_{EO} values provided in Table 2 using previously reported conductivity measurements on mixtures of PEO homopolymer and LiTFSI.[49,50] The ionic conductivity of LiTFSI and PEO homopolymer mixtures is independent of polymer molecular weight over the range of this study ($M_{n,PEO}$ of 2 to 4.2 kg/mol).[51] This justifies our use of a molecular-weight-independent value of σ_{EO} in eq 8. The values of $\sigma_{i,N}$ thus obtained at 90 °C are listed in Table 3. For well-connected lamellae, the expected value of f_i is 0.67. The reported values of $\sigma_{i,N}$ in Table 3 are less than this, an observation that is consistent with measurements of ionic conductivity of PS−PEO block copolymers in the low molecular weight limit.[43]

The electronic conductivity of P3HT−PEO block copolymers can be analyzed by a scheme similar to that described in the preceding paragraph. The normalized electronic conductivity of a block copolymer, $\sigma_{e,N}$, is defined as

$$\sigma_{e,N} = \frac{\sigma_e(r_0 = 0.085)}{\phi_{HT}\sigma_{HT}(r_{HT})} = \frac{\sigma_e(r_0 = 0)}{\phi_{HT}\sigma_{HT}(r_{HT} = 0)} \quad (9)$$

where ϕ_{HT} is the P3HT volume fraction, σ_e is the electronic conductivity of the block copolymer, and $\sigma_{HT}(r_{HT})$ is that of P3HT(5) homopolymer at salt concentration r_{HT} for each block copolymer given in Table 2. The second equality arises due to our approach for obtaining r_{HT}. As was the case with normalizing ionic conductivity, we assume that σ_{HT} is independent of P3HT molecular weight over the range of this study ($M_{n,P3HT}$ of 5 to 9 kg/mol). To our knowledge, the effect of molecular weight on conductivity, the product of charge carrier mobility and concentration, for bulk P3HT samples has not been reported. Previous work shows that changing $M_{n,P3HT}$ from 3 to 30 kg/mol results in a factor of 25 increase in mobility in a diode configuration[52] and a factor of 10 000 increase in mobility in a transistor configuration.[53] It is important to note that the reported mobilities are obtained from measurements on thin films (20−200 nm) and that the measured properties depend on substrate effects and processing conditions. Further work is thus required to determine the limitations of the proposed normalization procedure for electronic conductivity in block copolymers.

The values of $\sigma_{e,N}$ obtained from eq 9 are listed in Table 3. The values of $\sigma_{e,N}$ of P3HT−PEO(9−2) and P3HT−PEO(6−2) are significantly greater than unity. It is clear that in this case, $\sigma_{e,N}$ is not equal to the morphology factor, which by definition is less than unity. The $\sigma_{e,N}$ values listed in Table 3 should be interpreted as lower bounds for the increase in intrinsic electronic conductivity of P3HT microphases due to nanostructuring. Thus the intrinsic electronic conductivity of P3HT domains in P3HT−PEO(6−2) is at least a factor of 12 larger than that of P3HT(5) homopolymer. This factor is 8 for P3HT−PEO(9−2) and not significantly different from unity for P3HT−PEO(5−4) (Table 3). Note that the largest increase is obtained in the P3HT−PEO(6−2) sample, wherein the molecular weight of the P3HT block is closely matched to the P3HT homopolymer. The higher conductivity of the asymmetric block copolymers is unexpected due to the presence of the electronically insulating PEO microphase. Studies on poly(3-alkylthiophenes) (P3AT) and electronically insulating polymer composites have shown a similar increase in electronic conductivity at high P3AT weight fractions.[54−56] The results of these studies suggest that properties of the material surrounding the crystalline P3AT regions affect the electronic charge transport.[55]

It is important to note that the results in Tables 2 and 3 are based on the simplest possible interpretation of the available data. The factor by which conductivity of pure P3HT increases with added salt might be different from that obtained in P3HT-containing block copolymers. Note that the dependence of σ_e on ϕ_{HT} is nonmonotonic and presented on a logarithmic scale in Figure 9. This cannot be anticipated from eq 1, which predicts a monotonic (linear) increase of σ_e with increasing ϕ_{HT}.

CONCLUSIONS

We have explored the relationship between morphology and transport of both electronic and ionic charge in block copolymer/salt mixtures. SAXS experiments, used to determine morphology, indicate the presence of a lamellar phase in neat P3HT−PEO(5−4) at room temperature and a disordered phase at temperatures above 60 °C. In contrast, SAXS profiles of neat P3HT−PEO(6−2) and P3HT−PEO(9−2) are featureless, indicating that the morphology is dominated by P3HT nanofibrils. After the addition of LiTFSI at $r_0 = 0.085$, the SAXS profiles from all three samples contain signatures of microphase separation. At this concentration, SAXS profiles from P3HT−PEO(5−4)/LiTFSI mixtures contain clear signatures of a lamellar morphology at temperatures up to 90 °C, while SAXS profiles from P3HT−PEO(6−2)/LiTFSI and P3HT−PEO(9−2)/LiTFSI mixtures contain broad shoulders that cannot be interpreted in terms of specific morphologies.

A key difference between the present samples and those used in previous studies on charge transport in block copolymers[32,40,42,57,58] is both ionic and electronic charges are transported simultaneously in the

present system. A combination of ac impedance spectroscopy and dc measurements enables the determination of electronic and ionic conductivity in our samples. We discovered that the addition of LiTFSI to P3HT homopolymer results in an approximately 400-fold increase in electronic conductivity at high salt concentrations. By combining this result with measurements of electronic conductivity of P3HT–PEO copolymers with and without salt we estimated the extent to which LiTFSI partitions between the P3HT and PEO microphases. The ionic conductivities of P3HT–PEO/LiTFSI mixtures are lower than those of PEO/LiTFSI mixtures. This is expected due to the presence of the nonionically conducting P3HT microphases in the P3HT–PEO/LiTFSI mixtures (see eq 1). Neat P3HT–PEO copolymers transport only electronic charge. The electronic conductivities of the neat asymmetric P3HT–PEO copolymers are significantly higher than those of the P3HT homopolymer. This is unexpected because one expects the presence of the nonelectronically conducting PEO microphases in P3HT–PEO to result in a decrease in electronic conductivity (see eq 1). We hope to identify the reason for this observation in future work.

EXPERIMENTAL METHODS

Materials. Ethynyl-terminated poly(3-hexylthiophene) (ethynyl-P3HT) was synthesized using Grignard metathesis (GRIM) polymerization.[59] Azide-terminated PEO (Azide-PEO) (2000 g/mol) was purchased from Polymer Source. Azide-PEO (4200 g/mol) was obtained through end-group functionalization of monomethoxy-PEO[60] that was purchased from Polymer Source. The ethynyl-P3HT and azide-PEO were coupled using 1,3-dipolar cylcoaddition click reaction to yield P3HT–PEO block copolymer (refer to ref 39 for more details on synthesis and purification). The molecular weight and regioregularity of ethynyl-P3HT was determined using ^{1}H NMR. The polydispersity of the polymer was determined on a Viscotek GPC (gel permeation chromatography) instrument (TDA 302), a set of three Waters Styrogel HR columns (two HR3 and one HR4 column) and with tetrahydrofuran (THF) as the mobile phase (flow rate of 1 mL/min, 35 °C). The GPC was calibrated using polystyrene standards. Table 1 shows the polymers used in this study. P3HT(5) is an allyl-terminated homopolymer, which is also synthesized and purified in the same manner as ethynyl-P3HT.

Sample Preparation and Measurements. All of the steps used to make the P3HT–PEO/LiTFSI mixtures were conducted in argon-filled gloveboxes (MBraun and Vacuum Atmospheres). LiTFSI was purchased from Novolyte and dried under vacuum at 120 °C for 3 days to remove any residual water. Neat P3HT–PEO samples were dried under vacuum at 90 °C for 2–3 days before making salt samples. LiTFSI/dry-THF mixtures were prepared in a volumetric flask at a concentration of 0.5 g/mL. The P3HT–PEO samples were dissolved in dry benzene at a concentration of 5 mg/mL in scintillation vials. Heating the sample slightly using a heated stir plate helped the dissolution process. An appropriate amount of LiTFSI/dry-THF solution was added to the P3HT–PEO solution to obtain the desired salt concentration. The P3HT–PEO salt solutions were stirred overnight to ensure good mixing and placed in an airtight desiccator, which was transferred into a freeze-drying unit. The process ensured no exposure to air. PEO/LiTFSI and P3HT(5)/LiTFSI samples were prepared in a similar manner. We define r_0, the initial total salt concentration in the block copolymer, as the ratio between moles of LiTFSI and moles of EO units. We define r_{EO} as the ratio between moles of LiTFSI and moles of EO units. r_{HT} is the ratio between moles of LiTFSI and moles of 3-hexylthiophene unit.

Neat P3HT–PEO and P3HT–PEO/LiTFSI samples were pressed into 125 μm thick Garolite spacers and placed in an airtight sample holder with Kapton windows. The samples were annealed overnight under vacuum at 90 °C. Small-angle X-ray scattering and wide-angle X-ray scattering measurements were taken at the Advanced Light Source (ALS) beamline 7.3.3 at Lawrence Berkeley National Laboratory. A silver behenate sample was used as a standard for SAXS and aluminum standard for WAXS. The 2D scattering patterns were collected on an ADSC CCD detector or 1 M Pilatus detector. The scattering patterns were reduced using the Nika macro for Igor Pro developed by Jan Ilavsky at Argonne National Laboratory. The measured two-dimensional scattering data were averaged azimuthally to obtain intensity (I) *versus* magnitude of the scattering wave vector $q = 4\pi \sin(\theta/2)/\lambda$, where λ is the wavelength of the incident X-rays (0.124 nm) and θ is the scattering angle.

The sample for transmission electron microscopy was prepared by dip coating a copper grid in a P3HT–PEO/THF solution (10 mg/mL) and annealed at 100 °C overnight under vacuum. Bright-field TEM images were obtained using a Ziess LIBRA microscope operating at 200 kV. Contrast in the image arises from density differences between the P3HT-rich (dark) and PEO with LiTFSI (light) microphases.

Samples for electrochemical measurements were prepared by hot pressing freeze-dried samples into a 125 μm thick Garolite G-10 spacer with an inner-hole diameter of 3.88 mm. For thickness-dependent measurements on the P3HT–PEO/LiTFSI mixture, we also used a 250 μm G-10 spacer and a 25 μm Kapton spacer. Nickel foil current collectors were pressed at 1000 psi on both sides of the spacer at 90 °C for 30 s using a Carver press (in a glovebox). The Ni–polymer–Ni sandwich was allowed to anneal for an additional 30 min at 90 °C after the pressure was released. The actual thickness of the polymer in the spacer was measured after annealing. Due to overfilling the spacer hole, the actual thickness is slightly larger than the spacer thickness, but is not an issue for taking measurements, as the polymer is a hard solid at 90 °C. The sandwich was sealed in aluminum-laminated pouch material (Showa Denko) using a vacuum sealer (Packaging Aids Corp) with nickel tabs in an argon glovebox. Our approach ensures that the samples are air- and water-free.

The impedance spectroscopy measurements were made using either a Bio-Logics VMP3 or a Solartron 1260 instrument with applied ac voltages in the 10–50 mV range and frequencies ranging from 1 MHz to 1 mHz. Resistances were calculated from the complex impedance data ($Z^* = Z' - iZ''$), where Z' and Z'' are the real and imaginary impedances, respectively, using Nyquist plots ($-Z''$ *vs* Z'). The conductivity, σ, is given by

$$\sigma = \frac{L}{R} \tag{10}$$

where L is the polymer thickness and R is the resistance ($\Omega \cdot cm^2$), obtained from intersections of the Nyquist plots on the Z′ axis. Small dc potentials between −50 and 50 mV were imposed on the P3HT-containing samples, and the steady-state current response was measured using the Biologic VMP3 instrument. All conductivity measurements were averaged over a minimum of three samples, and all error bars were calculated from one standard deviation. All reported conductivity values are from ac impedance measurements unless stated otherwise.

Equivalent Circuit Curve Fitting. Experimental ac impedance spectroscopy data were analyzed using equivalent circuits composed of constant phase elements (CPE) and resistors. The impedance of a CPE is given by

$$Z_Q = \frac{1}{Q(i\omega)^a} \tag{11}$$

where Q is the capacitance (constant phase element), ω is the angular frequency, and a is a measure of nonideality of the capacitor. The unit for Q is $F \cdot s^{a-1}$. Both Q and a are fitting parameters, and $a = 1$ corresponds to the ideal capacitor. Physical arguments were used to arrive at a particular equivalent circuit, and the Randomize + Simplex algorithm built into the EC-Lab software package was used to fit the impedance data. In all cases, we report the parsimonious result, *i.e.*, the simplest equivalent circuit with the fewest elements that can describe the data.

Conflict of Interest: The authors declare no competing financial interest.

Acknowledgment. The measurement of electronic and ionic conductivities of the samples, which is the major portion of this work, was supported by a grant from the National Science Foundation (CBET 0966632). The polymer synthesis was supported the BATT program at Lawrence Berkeley National Laboratory, U.S. DOE Contract No. DE-AC02-05CH11231. SAXS experiments were performed at the Advanced Light Source, LBNL, a DOE national user facility supported by the DOE under the same contract. We gratefully acknowledge A. Teran for providing the PEO conductivity data, and R. Segalman and M. Jeffries-EL for helpful discussions.

REFERENCES AND NOTES

1. Feynman, R. P.; Leighton, R. B.; Sands, M. L. *The Feynman Lectures on Physics*, New Millennium ed.; Basic Books: New York, 2011.
2. Shockley, W.; Sparks, M.; Teal, G. P-N Junction Transistors. *Phys. Rev.* **1951**, *83*, 151–162.
3. Heeger, A. J. Semiconducting and Metallic Polymers: The Fourth Generation of Polymeric Materials (Nobel Lecture). *Angew. Chem., Int. Ed.* **2001**, *40*, 2591–2611.
4. Linden, D.; Reddy, T. B. *Handbook of Batteries*, 3rd ed.; McGraw-Hill: New York, 2002.
5. Riess, I. Mixed Ionic-Electronic Conductors - Material Properties and Applications. *Solid State Ionics* **2003**, *157*, 1–17.
6. Teraoka, Y.; Zhang, H. M.; Okamoto, K.; Yamazoe, N. Mixed Ionic-Electronic Conductivity of La1-Xsrxco1-Yfeyo3-Delta Perovskite-Type Oxides. *Mater. Res. Bull.* **1988**, *23*, 51–58.
7. Adler, S. B. Limitations of Charge-Transfer Models for Mixed-Conducting Oxygen Electrodes. *Solid State Ionics* **2000**, *135*, 603–612.
8. Adler, S. B.; Lane, J. A.; Steele, B. C. H. Electrode Kinetics of Porous Mixed-Conducting Oxygen Electrodes. *J. Electrochem. Soc.* **1996**, *143*, 3554–3564.
9. Riess, I. Measurements of Electronic and Ionic Partial Conductivities in Mixed Conductors, without the Use of Blocking Electrodes. *Solid State Ionics* **1991**, *44*, 207–214.
10. Riess, I. Review of the Limitation of the Hebb-Wagner Polarization Method for Measuring Partial Conductivities in Mixed Ionic Electronic Conductors. *Solid State Ionics* **1996**, *91*, 221–232.
11. Huggins, R. A. Simple Method to Determine Electronic and Ionic Components of the Conductivity in Mixed Conductors—A Review. *Ionics* **2002**, *8*, 300–13.
12. Jamnik, J.; Maier, J. Treatment of the Impedance of Mixed Conductors—Equivalent Circuit Model and Explicit Approximate Solutions. *J. Electrochem. Soc.* **1999**, *146*, 4183–4188.
13. Costantini, N.; Wegner, G.; Mierzwa, M.; Pakula, T. Simultaneous Ionic and Electronic Conductivity in Polymeric Materials. *Macromol. Chem. Phys.* **2005**, *206*, 1345–1354.
14. Witker, D.; Curtis, M. D. Lithium Ion and Electronic Conductivity in 3-(oligoethylene oxide)thiophene Comb-Like Polymers. *J. Power Sources* **2006**, *156*, 525–532.
15. Ren, X. M.; Pickup, P. G. Ionic and Electronic Conductivity of Poly(3-methylpyrrole-4-carboxylic acid). *J. Electrochem. Soc.* **1992**, *139*, 2097–2105.
16. Ren, X. M.; Pickup, P. G. Coupling of Ion and Electron-Transport during Impedance Measurements on a Conducting Polymer with Similar Ionic and Electronic Conductivities. *J. Chem. Soc., Faraday Trans.* **1993**, *89*, 321–326.
17. Plocharski, J.; Wycislik, H. Mixed Conductivity in Poly-(*p*-phenylene) Doped with Iron Chloride. *Solid State Ionics* **2000**, *127*, 337–344.
18. Siroma, Z.; Hagiwara, J.; Yasuda, K.; Inaba, M.; Tasaka, A. Simultaneous Measurement of the Effective Ionic Conductivity and Effective Electronic Conductivity in a Porous Electrode Film Impregnated with Electrolyte. *J. Electroanal. Chem.* **2010**, *648*, 92–97.
19. Sirringhaus, H.; Brown, P. J.; Friend, R. H.; Nielsen, M. M.; Bechgaard, K.; Langeveld-Voss, B. M. W.; Spiering, A. J. H.; Janssen, R. A. J.; Meijer, E. W.; Herwig, P.; *et al*. Two-Dimensional Charge Transport in Self-Organized, High-Mobility Conjugated Polymers. *Nature* **1999**, *401*, 685–688.
20. Yang, H. C.; Shin, T. J.; Yang, L.; Cho, K.; Ryu, C. Y.; Bao, Z. N. Effect of Mesoscale Crystalline Structure on the Field-Effect Mobility of Regioregular Poly(3-hexylthiophene) in Thin-Film Transistors. *Adv. Funct. Mater.* **2005**, *15*671–676.
21. Wang, G. M.; Swensen, J.; Moses, D.; Heeger, A. J. Increased Mobility from Regioregular Poly(3-hexylthiophene) Field-Effect Transistors. *J. Appl. Phys.* **2003**, *93*, 6137–6141.
22. Zhang, R.; Li, B.; Iovu, M. C.; Jeffries-El, M.; Sauve, G.; Cooper, J.; Jia, S. J.; Tristram-Nagle, S.; Smilgies, D. M.; Lambeth, D. N.; *et al*. Nanostructure Dependence of Field-Effect Mobility in Regioregular Poly(3-hexylthiophene) Thin Film Field Effect Transistors. *J. Am. Chem. Soc.* **2006**, *128*, 3480–3481.
23. McCullough, R.; Tristramnagle, S.; Williams, S.; Lowe, R.; Jayaraman, N. Self-Orienting Head-to-Tail Poly(3-alkylthiophenes)—New Insights on Structure-Property Relationships in Conducting Polymers. *J. Am. Chem. Soc.* **1993**, *115*, 4910–4911.
24. Tao, Y.; McCulloch, B.; Kim, S.; Segalman, R. A. The Relationship between Morphology and Performance of Donor-Acceptor Rod-Coil Block Copolymer Solar Cells. *Soft Matter* **2009**, *5*, 4219–4230.
25. Bondarev, D.; Zednik, J.; Sloufova, I.; Sharf, A.; Prochazka, M.; Pfleger, J.; Vohlidal, J. Synthesis and Properties of Cationic Polyelectrolyte with Regioregular Polyalkylthiophene Backbone and Ionic-Liquid Like Side Groups. *J. Polym. Sci., Part A: Polym. Chem.* **2010**, *48*, 3073–3081.
26. Chen, T. A.; Wu, X. M.; Rieke, R. D. Regiocontrolled Synthesis of Poly(3-alkylthiophenes) Mediated by Rieke Zinc—Their Characterization and Solid-State Properties. *J. Am. Chem. Soc.* **1995**, *117*, 233–244.
27. Kuila, B. K.; Malik, S.; Batabyal, S. K.; Nandi, A. K. *In-Situ* Synthesis of Soluble Poly(3-hexylthiophene)/Multiwalled Carbon Nanotube Composite: Morphology, Structure, and Conductivity. *Macromolecules* **2007**, *40*, 278–287.
28. Liu, C.; Oshima, K.; Shimomura, M.; Miyauchi, S. Anisotropic Conductivity-Temperature Characteristic of Solution-Cast Poly(3-hexylthiophene) Films. *Synth. Met.* **2006**, *156*, 1362–1367.
29. Obrzut, J.; Page, K. A. Electrical Conductivity and Relaxation in Poly(3-hexylthiophene). *Phys. Rev. B* **2009**, *80*.
30. Pal, S.; Roy, S.; Nandi, A. K. Temperature Variation of Dc Conductivity of Poly(3-alkyl thiophenes) and Their Cocrystals. *J. Phys. Chem. B* **2005**, *109*, 18332–18341.
31. McCullough, R. D. The Chemistry of Conducting Polythiophenes. *Adv. Mater.* **1998**, *10*, 93–116.
32. Liu, J. S.; Sheina, E.; Kowalewski, T.; McCullough, R. D. Tuning the Electrical Conductivity and Self-Assembly of Regioregular Polythiophene by Block Copolymerization: Nanowire Morphologies in New Di- and Triblock Copolymers. *Angew. Chem., Int. Ed.* **2002**, *41*, 329–332.
33. Guoying, C.; Richardson, T. J. Overcharge Protection for Rechargeable Lithium Batteries Using Electroactive Polymers. *Electrochem. Solid-State Lett.* **2004**, *7*, A23–A26.
34. Schopf, G.; Kossmehl, G. Polythiophenes—Electrically Conductive Polymers. In *Advances in Polymer Science*; Springer: Berlin, 1997; Vol. 129, pp 3—145.
35. Iovu, M. C.; Craley, C. R.; Jeffries-El, M.; Krankowski, A. B.; Zhang, R.; Kowalewski, T.; McCullough, R. D. Conducting Regioregular Polythiophene Block Copolymer Nanofibrils Synthesized by

Reversible Addition Fragmentation Chain Transfer Polymerization (RAFT) and Nitroxide Mediated Polymerization (NMP). *Macromolecules* **2007**, *40*, 4733–4735.
36. Iovu, M. C.; Jeffries-El, M.; Sheina, E. E.; Cooper, J. R.; McCullough, R. D. Regioregular Poly(3-alkylthiophene) Conducting Block Copolymers. *Polymer* **2005**, *46*, 8582–8586.
37. Iovu, M. C.; Zhang, R.; Cooper, J. R.; Smilgies, D. M.; Javier, A. E.; Sheina, E. E.; Kowalewski, T.; McCullough, R. D. Conducting Block Copolymers of Regioregular Poly(3-hexylthiophene) and Poly(methacrylates): Electronic Materials with Variable Conductivities and Degrees of Interfibrillar Order. *Macromol. Rapid Commun.* **2007**, *28*, 1816–1824.
38. Lee, Y.-H.; Yen, W.-C.; Su, W.-F.; Dai, C.-A. Self-Assembly and Phase Transformations of [Small Pi]-Conjugated Block Copolymers That Bend and Twist: From Rigid-Rod Nanowires to Highly Curvaceous Gyroids. *Soft Matter* **2011**, *7*, 10429–10442.
39. Javier, A. E.; Patel, S. N.; Hallinan, D. T.; Srinivasan, V.; Balsara, N. P. Simultaneous Electronic and Ionic Conduction in a Block Copolymer: Application in Lithium Battery Electrodes. *Angew. Chem., Int. Ed.* **2011**, *50*, 9848–9851.
40. Singh, M.; Odusanya, O.; Wilmes, G. M.; Eitouni, H. B.; Gomez, E. D.; Patel, A. J.; Chen, V. L.; Park, M. J.; Fragouli, P.; Iatrou, H.; *et al*. Effect of Molecular Weight on the Mechanical and Electrical Properties of Block Copolymer Electrolytes. *Macromolecules* **2007**, *40*, 4578–4585.
41. Mullin, S. A.; Stone, G. M.; Panday, A.; Balsara, N. P. Salt Diffusion Coefficients in Block Copolymer Electrolytes. *J. Electrochem. Soc.* **2011**, *158*, A619–A627.
42. Panday, A.; Mullin, S.; Gomez, E. D.; Wanakule, N.; Chen, V. L.; Hexemer, A.; Pople, J.; Balsara, N. P. Effect of Molecular Weight and Salt Concentration on Conductivity of Block Copolymer Electrolytes. *Macromolecules* **2009**, *42*, 4632–4637.
43. Wanakule, N. S.; Panday, A.; Mullin, S. A.; Gann, E.; Hexemer, A.; Balsara, N. P. Ionic Conductivity of Block Copolymer Electrolytes in the Vicinity of Order-Disorder and Order-Order Transitions. *Macromolecules* **2009**, *42*, 5642–5651.
44. Yang, X.; Loos, J.; Veenstra, S.; Verhees, W.; Wienk, M.; Kroon, J.; Michels, M.; Janssen, R. Nanoscale Morphology of High-Performance Polymer Solar Cells. *Nano Lett.* **2005**, *5*, 579–583.
45. Eitouni, H. B.; Balsara, N. P. Thermodynamics of Polymer Blends. In *Physical Properties of Polymers Handbook*; Mark, J. E., Ed.; Springer: New York, 2007; pp 339−356.
46. Guo, X.; Fleig, J.; Maier, J. Separation of Electronic and Ionic Contributions to the Grain Boundary Conductivity in Acceptor-Doped $SrTiO_3$. *J. Electrochem. Soc.* **2001**, *148*, J50–J53.
47. Bruce, P. G.; Gray, F. M.; Shi, J.; Vincent, C. A. Ionic Transport in Polymer Electrolytes. *Philos. Mag. A* **1991**, *64*, 1091–1099.
48. Likun, P.; Zhuo, S. Solvent and Temperature-Dependent Conductive Behavior of Poly(3-hexylthiophene). *J. Phys. Chem. Solids* **2009**, 70.
49. Lascaud, S.; Perrier, M.; Vallee, A.; Besner, S.; Prudhomme, J.; Armand, M. Phase-Diagrams and Conductivity Behavior of Poly(ethylene oxide) Molten-Salt Rubbery Electrolytes. *Macromolecules* **1994**, *27*, 7469–7477.
50. Conductivity for PEO homopolyer/LiTFSI mixtures was taken from published data by Lascaud *et al*. (ref 49). The PEO molecualar weight was approximately 4 kg/mol. The ionic conductivity at 90 °C was interpolated for each LiTFSI salt concentration in the PEO microphase (see Table 2).
51. Teran, A. A.; Tang, M. H.; Mullin, S. A.; Balsara, N. P. Effect of Molecular Weight on Conductivity of Polymer Electrolytes. *Solid State Ionics* **2011**, *203*, 18–21.
52. Goh, C.; Kline, R. J.; McGehee, M. D.; Kadnikova, E. N.; Frechet, J. M. J. Molecular-Weight-Dependent Mobilities in Regioregular Poly(3-hexyl-thiophene) Diodes. *Appl. Phys. Lett.* **2005**, 86.
53. Kline, R. J.; McGehee, M. D. Morphology and Charge Transport in Conjugated Polymer. *Polym. Rev.* **2006**, *46*, 27–45.
54. Lu, G.; Tang, H.; Qu, Y.; Li, L.; Yang, X. Enhanced Electrical Conductivity of Highly Crystalline Polythiophene/Insulating-Polymer Composite. *Macromolecules* **2007**, *40*, 6579–6584.
55. Lu, G.; Tang, H.; Huan, Y.; Li, S.; Li, L.; Wang, Y.; Yang, X. Enhanced Charge Transportation in Semiconducting Polymer/Insulating Polymer Composites: The Role of an Interpenetrating Bulk Interface. *Adv. Funct. Mater.* **2010**, *20*, 1714–1720.
56. Goffri, S.; Muller, C.; Stingelin-Stutzmann, N.; Breiby, D.; Radano, C.; Andreasen, J.; Thompson, R.; Janssen, R. Nielsen, M.; Smith, P.; *et al*. Multicomponent Semiconducting Polymer Systems with Low Crystallization-Induced Percolation Threshold. *Nat. Mater.* **2006**, *5*, 950–956.
57. Dante, M.; Yang, C.; Walker, B.; Wudl, F.; Nguyen, T.-Q. Self-Assembly and Charge-Transport Properties of a Polythiophene-Fullerene Triblock Copolymer. *Adv. Mater.* **2010**, *22*, 1835–1839.
58. Kumar, A.; Baklar, M.; Scott, K.; Kreouzis, T.; Stingelin-Stutzmann, N. Efficient, Stable Bulk Charge Transport in Crystalline/Crystalline Semiconductor-Insulator Blends. *Adv. Mater.* **2009**, *21*, 4447–4451.
59. Jeffries-El, M.; Sauve, G.; McCullough, R. D. *In-Situ* End-Group Functionalization of Regioregular Poly(3-alkylthiophene) Using the Grignard Metathesis Polymerization Method. *Adv. Mater.* **2004**, *16*, 1017–1019.
60. Parrish, B.; Breitenkamp, R.; Emrick, T. PEG- and Peptide-Grafted Aliphatic Polyesters by Click Chemistry. *J. Am. Chem. Soc.* **2005**, *127*, 7404–7410.